CONDENSATION OF REFRIGERANT R-407C INSIDE HORIZONTAL FINNED TUBES

Agung Tri Wijayanta[1]

ABSTRACT

This paper provides plan experiment of heat transfer and pressure drop during condensation of refrigerant R-407C inside horizontal finned tubes. The substitution of traditional refrigerants, and particularly of R-22 (chlorodifluoromethane), can call for the use of zeotropic mixtures of HFCs with zero ODP (ozone depleting potential). R-407C is one of the replacement candidates for R-22. Due to its zeotropic nature, the heat transfer coefficient during condensation of R-407C inside a horizontal tube is much lower than that for R-22. Various types of finned tubes have been developed to enhance condensation of refrigerants inside horizontal tubes. However, no theoretical model is currently available that can be used to optimize the fin geometry for condensation of R-407C. The goal of the research is to develop a theoretical model for predicting the heat transfer and to develop an empirical correlation for the pressure drop during condensation of R-407C inside a horizontal finned tube.

Keywords: heat transfer, pressure drop, condensation, R-407C, finned tubes

INTRODUCTION

R-407C is a mixture of 23 % of R-32, 25 % of R-125 and 52 % of R-134a. The physical properties of R-407C is similar to that for R-22 except for the fact that it is a zeotropic mixture. It has a temperature glide (temperature difference between the dew-point and bubble-point) of about 6 K. While these characteristics can be used to improve thermodynamic cycle performance, it also acts to deteriorate the heat transfer performance of evaporators and condensers. The properties of R-22 and R-407C show in Table 1 (Kuo and Wang, 1996).

Table 1 : The Properties of R-22 and R-407C

Property	R 22	R-407C
P_{sat} (kPa)	600	600
T_{sat} (°C)	6.04	1.66
ρ_r (kg/m^3)	1262	1246
ρ_g (kg/m^3)	25.66	25.03
Cp_r (kJ/kg K)	1.214	1.377
Cp_g (kJ/kg K)	0.7896	0.8722
i_{fg} (kJ/kg)	197.8	215.4
μ_r (10^{-6} N s/m^2)	12.03	11.83
μ_g (10^{-6} N s/m^2)	207.7	219.6
k_g (mW/m K)	9.7	11.9
k_f (mW/m K)	99.62	102.0

Internal flow is encountered in numerous applications, and important to appreciate its unique features. Many internal flow problems involve heat transfer in a concentric tube annulus (Wijayanta, 1994; 1995). Fluid passes through the space formed by the concentric tubes, and convection heat transfer may occur to or from both the inner and outer tube surfaces.

The refrigeration and air conditioning industry is developing very compact machinery, and this requires the use of heat exchangers with enhanced surfaces. Air cooled condensers for

[1] Teaching staff at Mechanical Engineering Department, Sebelas Maret University, Surakarta.

refrigeration and heat pumps are manufactured with enhanced surfaces both on the external and on the refrigerant side.

New promising enhanced surfaces are now under scrutiny, such as herringbone heat transfer tubes (Ebisu et al., 1998; Miyara et al., 2000; Cavallini, et al., 2000), while microfin and cross-grooved tubes have already been used widely as they ensure a large heat transfer enhancement with a relatively low pressure drop increase. Typical microfin tubes available for industrial applications are made of copper and have an outside diameter from 4 to 15 mm, a single set of 50-70 spiral fins with spiral angle from 6° to 30°, fin height from 0.1 to 0.25 mm, triangular or trapezoidal fin shapes with an apex angle from 25° to 90°. Fig. 1 presents the characteristic geometrical parameters of microfin enhanced tubes.

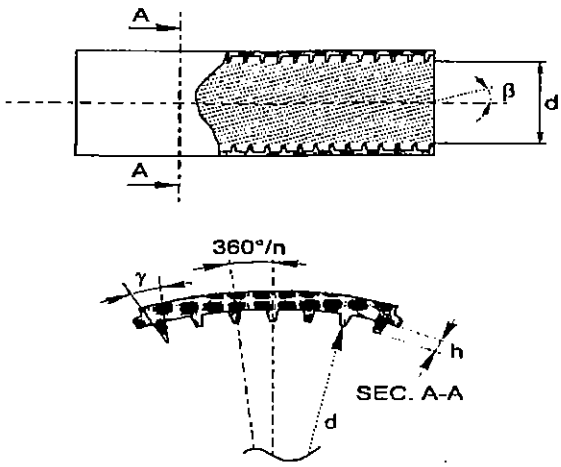

Fig. 1. Characteristic geometrical parameters of inside enhanced tubes

Cross-grooved tubes present an additional set of grooves at the same spiral angle, but an opposite angular direction to the first set. Cross-grooved tubes exhibit a higher heat transfer performance and also a higher pressure drop than microfin tubes. A comparison between typical microfin and cross-grooved surfaces is given in Fig. 2.

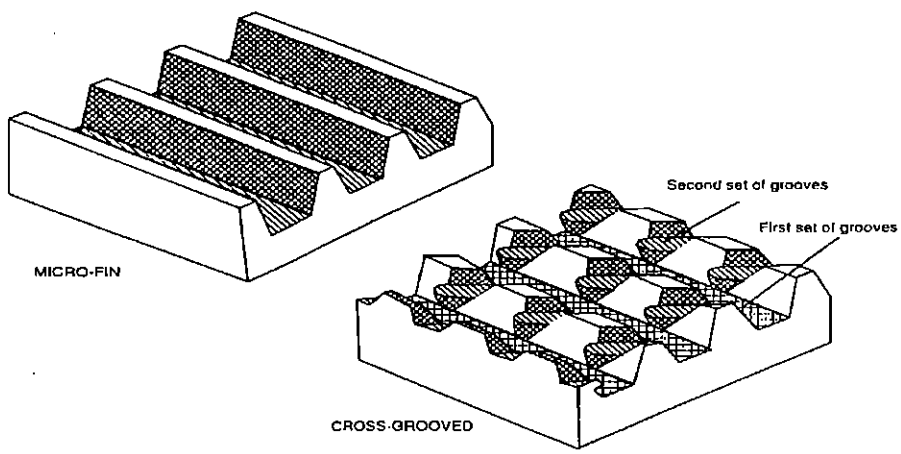

Fig. 2. Typical configuration of microfin and cross-grooved surfaces

Generally speaking, microfin tubes show a heat transfer enhancement, compared to equivalent smooth tubes under the same operating conditions, from 80 to 180% and over, with a pressure loss increase from 20 to 80%. Cross-grooved tubes give a 25-30% higher heat transfer performance than microfin tubes with a pressure drop only 6-10% higher. Heat transfer and pressure drop enhancements are partly due to the simple increase in the

effective exchange area, and additionally to the turbulence induced in the liquid film by the microfins and to the surface tension effect on the condensate drainage.

Muzzio et al. (1998) tested R-22 in a microfin tube with a new cross-section profile; the tube is characterized by a reduced number of fins with a sharp shape and two different heights, 0.23 and 0.16 mm, as shown in Fig. 3, with an apex angle of 40° and spiral angle 18°. The tube shows 10-20% higher heat transfer coefficients and the same pressure drop as conventional microfin tubes.

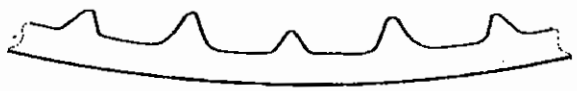

Fig. 3. Shape of Muzzio et al. (1998) microfin tube

Ebisu et al. (1998) tested a herringbone heat transfer tube with R-22 and R-407C, and compared its performance with an inner grooved tube, at the same operative conditions. The new tube is fabricated by embossing a flat strip of copper to form the desired geometry; the strip is then rolled into a round tube and welded. Fig. 4 illustrates the geometry of the strip: it has a pair of groove patterns, like herringbone. The tested herringbone tube showed a heat transfer enhancement, compared to the microfin tube under the same operating conditions [mass velocities from 200 to 500 kg/(m^2 s)], up to 200%, due to the increase in inside surface area (around 30%) and to the particular wetting in two different directions by V shape grooves, resulting in a film layer on both sides of the tube thinner than at the top and bottom, as shown in Fig. 4.

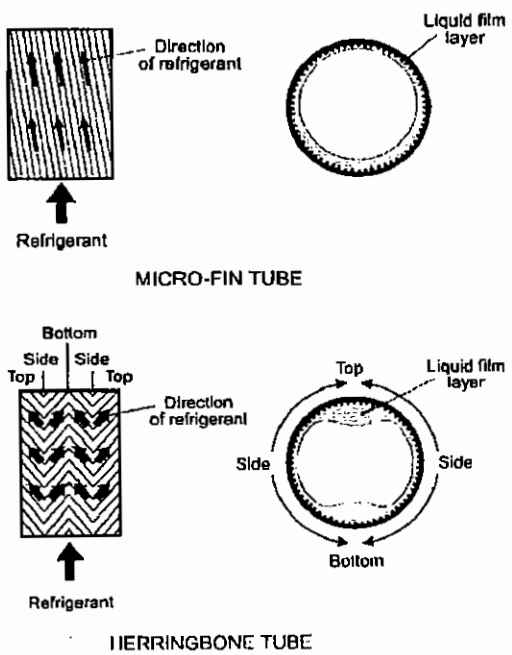

Fig. 4. Comparison between microfin and herringbone tubes in annular-type flow pattern

The pressure loss increase compared to the microfin tube is around 30% and reaches 50% at the highest refrigerant flow rate tested. The pressure drop increase is probably due to the higher fin height and surface area than the inner grooved tube.

Miyara et al. (2000) also tested condensation heat transfer and pressure drop of R-410A and R-22 in a herringbone type microfin tube and visually observed gas-liquid flow patterns in the tube. The authors report that the heat transfer coefficient and pressure drop of the herringbone tube is higher than that of a conventional helical microfin in the high mass

velocity region [G ≥ 300 kg/(m² s), vapor quality x > 0.25)], while it is slightly lower or equal in the low mass velocity region [G = 100 kg/(m² s)]. The authors suggest that the herringbone microfins work to remove liquid from both sides of the tube and collect it to its top and bottom part. This action is effective only in the high mass velocity region, especially at high vapor quality. In the low mass velocity region and at low quality the liquid flows mainly in the bottom part of the tube.

EXPERIMENTAL APPARATUS AND PROCEDURE

The experimental apparatus has been designed at Cooling Technology Laboratory, Institute of Advanced Material Study, Kyushu University, Japan. The experimental apparatus, shown schematically in Fig. 5, consists of forced circulation loops of test fluid and cooling water. The vapor generated in an electrically heated boiler [1] flows through superheaters [2], a mixing chamber [3] and a sight glass [4] to a test section [5]. The vapor condenses almost completely in the test section, and the condensate flows downward through a condensate receiver [6], then through a circulation pump [7], a flow control valve [8], and a strainer [9], and returns to the boiler. The loop is insulated thermally with fiberglass. The cooling water is pumped from a cooling water tank [10] by a feed water pump [11] to the test section through a calibrated rotameter [12]. After exchanging heat with the test fluid, the cooling water returns to the tank. The cooling water temperature at the test section inlet is regulated by a chiller [13] and a heater [14].

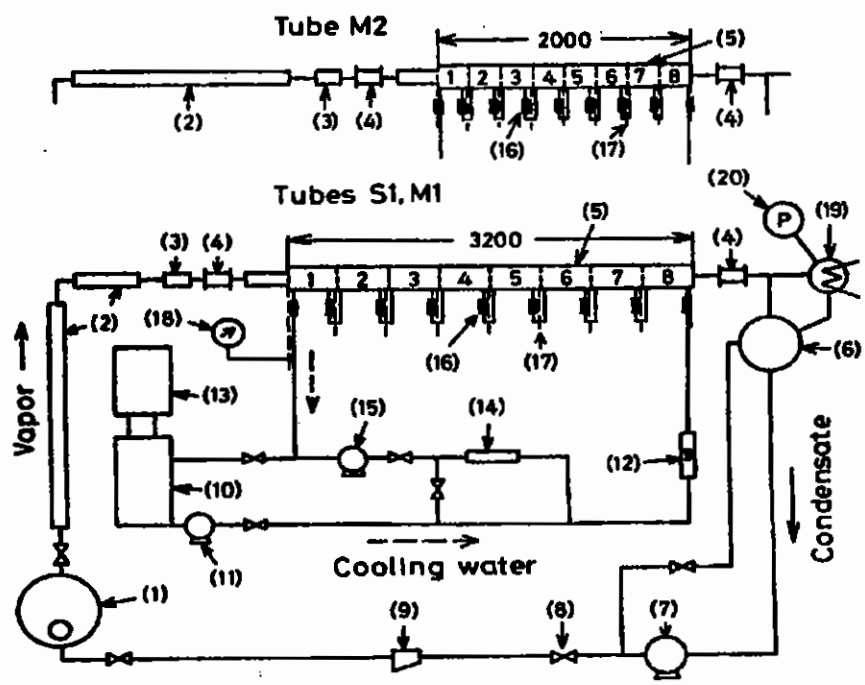

1. Boiler
2. Superheater
3. Mixing chamber
4. Sight glass
5. Test section
6. Condensate receiver
7. Circulation pump
8. Needle valve
9. Strainer
10. Cooling water tank
11. Feed water pump
12. Rotameter
13. Chiller
14. Feed water heater
15. Feed water pump
16. Mixing chamber
17. Pressure tap
18. Pressure gauge
19. Dump condenser
20. Vacuum pump

Fig. 5. Schematic diagram of experimental apparatus

Table 2 Dimensions of test tubes

Tube designation	S1	M1	M2
Outside diameter (mm)	7.00	7.00	7.00
Fin root diameter d_r (mm)	6.50	6.49	6.48
Fin height h_f (mm)	-	0.24	0.16
Average fin thickness t_m (mm)	-	0.20	0.19
Fin apex angle θ (rad)	-	1.10	1.52
Number of fins n	-	50	50
Helix angle Υ (deg)	-	13.0	15.0
Area enhancement ratio	1.00	1.49	1.32
Tube length (mm)	3200	3200	2000

The test section is a horizontal double-tube type heat exchanger with the vapor condensing in the inner copper tube and the cooling water passing counter currently through the annulus (Honda et al., 1998; 2000). A smooth tube and two microfin tubes, each having an outer diameter of about 7.0 mm, are used as the test tubes. The dimensions of the test tubes are listed in Table 2, where Tube S1 is a smooth tube and Tubes M1 and M2 are microfin tubes. Closeups of Tubes M1 and M2 are shown in Fig. 6. Lengths of the test sections are 3.2 m for Tubes S1 and M1, and 2.0 m for Tube M2.

Tube M1 Tube M2

Fig. 6. Cross-sections of Tubes M1 and M2.

To measure the axial distributions of heat transfer rate, tube wall temperature and static pressure, the test section is equipped with nine spacers to subdivide the annulus into eight equivalent subsections, which are referred to as the first, second, ..., and eighth subsections from the vapor inlet. Illustration of a subsection is shown in Fig. 7. For the test sections with Tubes S1 and M1, the outer duct is made of polyvinyl chloride pipe with inner diameter of 16.0 mm, and the length of the subsection Δl is 0.4 m. For the test section with Tube M2, on the other hand, the outer duct is made of polyvinyl chloride plate and is constructed to form the annulus with a diameter of 16.0 mm, and the value of Δl is 0.25 m. Each subsection are provided with cooling water inlet and outlet, and a mixing chamber is located between adjoining subsections to provide reliable data on the axial variation of the cooling water temperature T_c through the test section. The same type mixing chambers are also installed at both ends of the test section.

For Tubes S1 and M1, average wall temperature of each subsection T_{wm} is calculated from the local wall temperatures measured at seven points, spaced axially in groups of two or five. As shown in Fig. 7, in a cross-section of 0.1 m downstream from the subsection inlet, two fine grooves are cut on the outer surface of the inner tube at circumferential angles of φ and $\pi/2$ and $3\pi/2$ rad from the tube top. In the other cross-section of 0.3 m downstream from the inlet, fine grooves are machined at five angles of $\varphi = 0$; $\pi/2$, $3\pi/4$, $\pi/2$, and $3\pi/2$ rad. Teflon-coated, 0.127-mm-diameter constantan wires with bare tips are soldered in these grooves. This allows seven wall thermocouples between the constantan wires and the inner copper tube itself. These wires are passed through a small hole on the outer tube. For Tube M2, on the other hand, T_{wm} is measured by resistance thermometry. The inner tube is electrically insulated from the test loop, and the inner tube and a standard resistor (1 mΩ)

are connected in series by a lead wire to a DC power supply, and a constant current of 30 A is passed through the circuit. Copper-wires are soldered to the outer surface of the inner tube at the same positions of the spacers, and are passed through small holes on the outer duct. The calibration curve of the resistance-temperature relation is obtained by preliminary experiments.

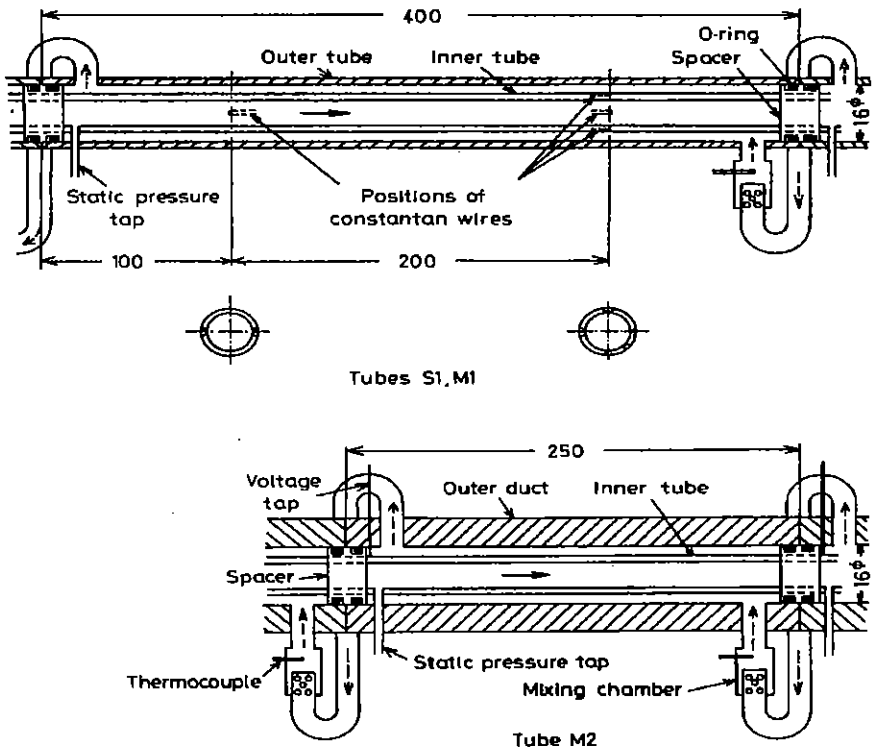

Fig. 7. Illustration of condensing section.

Static pressure at the vapor inlet P_{in} is measured by a precision Bourdon tube, reading to 10^3 Pa gauge, and a Fortin barometer. Eight pressure taps with 1-mm-diameter holes are drilled through the bottom of the inner tube at the inlet of each subsection, and a same type pressure tap is also installed at the exit of the test section. The adjoining pressure taps are connected to inverse U-tube manometers, reading to 1 mm, to measure the difference in condensate level. The mixed mean temperatures of the cooling water and the test fluid temperatures at the vapor inlet and in the strainer are measured by 1-mm-diameter type-K sheathed thermocouples. Cooling water flow rate is measured by a calibrated rotameter.

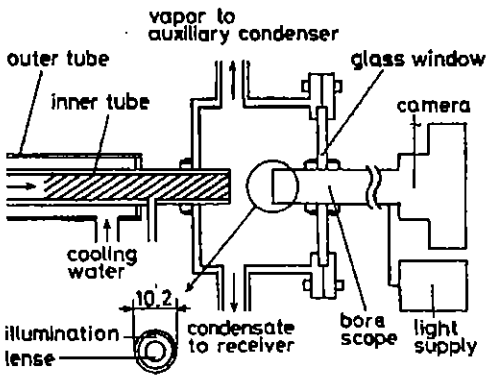

Fig. 8. Details of flow observation device attached to Tube M1

For Tube M1, behavior of condensate in the inner tube is observed using an industrial borescope installed at the tube exit. Fig. 8 illustrates the observation devices. The forward-viewing type scope with outer diameter of 10.2 mm, connected to a still camera and a light supply, is set coaxially to the inner tube. Tip of the scope are concentrically provided with a lens and an illumination and is located just downstream of the tube exit. This allows observation of the cross-sectional view of the condensate flow approaching the tube exit.

After the steady state is reached, the thermocouple outputs and the voltage drops of Tube M2 and the standard resistor are read five times to 1 μV using a data acquisition system. To avoid the effect of parasitic voltage, readings of the voltage drops are repeated by reversing the DC current and the averages of the two measurements are adopted as the experimental data.

DISCUSSION

Experiments will be conducted using R-407C as the test fluid. For each test run, the static pressure and the degree of vapor superheat, both at the vapor inlet, are maintained at 0.17 MPa ($T_i \equiv 313K$) and less than 2 K, respectively. The mass velocity of the test fluid G is obtained from the heat balance of the boiler by application of a steady flow energy balance for the test fluid (Honda et al., 2000) as:

$$G = \frac{4\left(Q_b - Q_l\right)}{\pi d_n^2 \left(i_{in} - i_{st}\right)} \tag{1}$$

where Q_b is the heat input to the boiler, Q_l is the heat loss from the boiler to the surroundings, and i_{in} and i_{st} are the specific enthalpies of the test fluid at the vapor inlet and in the strainer, respectively. d_n is the nominal diameter of the test tube, where the inner diameter d_i is adopted for Tube S1, and fin root diameter d_r for Tubes M1 and M2. The Q_l value was estimated on the assumption of one-dimensional heat conduction through the insulating material. The Q_l/Q_b value is estimated to be less than 0.02. The G value ranges from 80 to 460 kg/(m^2 s). For the observation study, the vapor mass quality at the tube exit is changed in three steps for a few prescribed values of G. The dump condenser was operated during the observations.

Average heat flux for a subsection q_n is defined on the basis of the nominal surface area (surface area of a smooth tube with d_n) as:

$$q_n = \Delta Q / \left(\pi d_n \Delta l\right)$$
$$\alpha_n = q_n / \left(T_s - T_w\right) \tag{2}$$

where ΔQ is the heat transfer rate in the subsection obtained from the temperature rise and flow rate of the cooling water. The vapor mass quality x is calculated successively from the vapor inlet, on the assumption of negligible condensate sub-cooling, using the values of G and ΔQ

In the data reduction, properties of the condensate and vapor are evaluated at the reference temperatures of $[T_w + 0.3(T_s-T_w)]$ and saturation temperature Ts, respectively. The properties are obtained from the JSME Data Book (1982). T_s corresponds to the measured vapor pressure and is obtained from the JSME Data Book, and T_w is the wall temperature at the fin root obtained from T_{wm}, making a small correction (less than 0.7 K) for radial wall conduction. Referring to Eq. (2), the uncertainty of α_n is affected by that of ΔQ and (T_s-T_w). The value of ΔQ is obtained from the temperature rise and flow rate of the cooling water, each having uncertainties of 0.05 K and ± 2% (Honda et al., 2000) .

Flow characteristics of condensate in a horizontal microfin tube will become more complex than in a horizontal smooth tube. This may be caused by the microfins, i.e., the condensate formed on a fin surface is drained by combined surface tension and gravity forces into the

groove, then the condensate is driven through the groove by the vapor shear force in the downstream direction. Effect of gravity force may be negligible in comparison with the other two forces in a high vapor velocity region. In a low vapor mass quality region, on the other hand, stratification of the condensate due to the gravity force may occur in the lower part of the tube as was observed in a horizontal smooth tube

The experimental data for tube S1 are compared with the recommendation equation of a smooth tube for obtaining reliability of the apparatus and measurements. The heat transfer coefficient as for a smooth tube recommended by Haraguchi (1994) and Fujii (1995) is expressed as

$$\alpha_s = \lambda_l \mathrm{Nu}_d / d_n \tag{3}$$

where :

$$\mathrm{Nu}_d = (\mathrm{Nu}_d)_v \quad \text{for } (\mathrm{Nu}_d)_v \geq (\mathrm{Nu}_d)_g \tag{4.a.}$$

$$\mathrm{Nu}_d = (\mathrm{Nu}_d)_g \quad \text{for } (\mathrm{Nu}_d)_v < (\mathrm{Nu}_d)_g \tag{4.b.}$$

$(\mathrm{Nu}_d)_v$ and $(\mathrm{Nu}_d)_g$ denote the Nusselt numbers in the shear-controlled and gravity-controlled regimes, respectively. Expressions for $(\mathrm{Nu}_d)_v$ and $(\mathrm{Nu}_d)_g$ are given by :

$$\left(\mathrm{Nu}_d\right)_v = 0.0125\left(\mathrm{Re}_l \sqrt{\rho_l / \rho_v}\right)^{0.9} \left(X/(1-X)\right)^{0.1X+0.8} \mathrm{Pr}_l^{0.63} \tag{5.a.}$$

$$\left(\mathrm{Nu}_d\right)_g = 0.725\left(\frac{\mathrm{Ga\,Pr}_l}{\mathrm{Ph}}\right)^{0.25} \frac{\left\{1+0.003\sqrt{\mathrm{Pr}_l}\, a^{3.1-0.5/\mathrm{Pr}_l}\right\}^{0.3}}{(1-bc)^{0.25}} \tag{5.b.}$$

a, *b*, and *c* are expressed as

$$a = \frac{0.47\sqrt{\rho_l / \rho_v}\left(\mathrm{Ph/Pr}_l\right)^{1/12}\left(\mathrm{Re}_l X/(1-X)\right)^{0.9}}{\left(\mathrm{Ga\,Pr}_l/\mathrm{Ph}\right)^{1.1/4}} \tag{5.c.}$$

$$b = \frac{1.55\left\{1+1.6\mathrm{x}10^{11}\left(\mathrm{Ph/Pr}_l\right)^5\right\}^{0.25}}{\sqrt{\rho_l / \rho_v}} \left\{\frac{\left(\mathrm{Ga\,Pr}_l/\mathrm{Ph}\right)^{0.25}}{\left(\mathrm{Re}_l X/(1-X)\right)}\right\}^{1.8} \tag{5.d.}$$

$$c = 40\exp\left\{-2.6\mathrm{x}10^{-4}\,\mathrm{Re}_l/(1-X)\right\} \tag{5.e.}$$

where :

the Galileo number	$\mathrm{Ga} = g d_n^3 / \nu_l^2$	(5.f.)
the phase change number	$\mathrm{Ph} = c_{pl}\,\Delta T / h_{fg}$	(5.g.)
the liquid Reynolds number	$\mathrm{Re}_l = G(1-X) d_n / \mu_l$	(5.h.)
the vapor-to-wall temperature difference	$\Delta T = T_s - T_w$	(5.i.)

The measured heat transfer coefficients for tube S1 are found by the prediction of Eq. (3) to have a mean absolute deviation of 10.3 percent. This indicates the reliability of the apparatus and measurements.

The heat transfer model proposed assumes that all the condensate flows through the fins with smooth liquid-vapor interface, since the objective of the present analysis is the prediction of condensation heat transfer in the annular flow regime. The condensate profile between adjacent fins depends on the combination of the fin geometry and condensate flow rate. Simplifying assumptions are introduced that permit fundamental assessment of the heat transfer rate:

1. The condensate flow is laminar
2. The wall temperature T_w is uniform
3. The inertia term in the momentum equation and the convection term in the energy equation can be neglected
4. The effect of gravity force can be neglected.

The procedure for heat transfer formulation of the problem is basically similar to the previous case reported by Honda et al. (2000). The experimental data for tube M1 and tube M2 are compared with recommendation equation to develop the model. The average Nusselt number for the fins surface (Nu_{pm}) and the average Nusselt number for the microfin tube (Nu_d), respectively, are given by:

$$Nu_{pm} = \alpha_m p/\lambda_l \quad (6.a.)$$

$$Nu_d = \alpha_n d_n/\lambda_l \quad (6.b.)$$

$$Nu_d = Nu_{pm}\,(d_n/p) \quad (6.c.)$$

For given conditions of vapor, tube and wall heat flux, the $(-dP/dz)_F$ value is obtained by executing the following procedure (Honda et al.,1998).

1. Calculate $(-dP/dz)_v$.

$$\left(-\frac{dP}{dz}\right)_v = \frac{2 f_v \rho_v u_{vs}^2}{d_n} \quad (7)$$

where :

$$f_v = 0.046\,\mathrm{Re}^{-0.2}\,\frac{d_n}{d_h}\sqrt{\frac{A_{fs}}{A_{fin}}}\,(\sec\gamma)^{0.75} \quad (8)$$

2. Calculate X_{tt} and Fr, respectively, then obtain • value.

$$X_{tt} = \left(\frac{1-x}{x}\right)^{0.9}\left(\frac{\mu_l}{\mu_v}\right)^{0.1}\left(\frac{\rho_v}{\rho_l}\right)^{0.5} \quad (9)$$

$$\mathrm{Fr} = \frac{Gx}{\sqrt{\rho_v(\rho_l-\rho_v)d_i g}} \quad (10)$$

$$\xi = 1+\eta\left(25X_{tt}^{0.8}+1.6X_{tt}^{2}\right) \quad (11)$$

where :

for smooth tube $\eta = \left(1+12/\mathrm{Fr}^{1.5}\right)^{-0.5}$ (12.a.)

for fin tube $\eta = \left(1+10/\mathrm{Fr}^{1.5}\right)^{-0.5}$ (12.b.)

3. Calculate •, then obtain ς value.

$$\beta = \left\{1+\frac{1-x}{x}\sqrt{\frac{\rho_v}{\rho_l}}\right\}^{-1} \quad (13)$$

$$\varsigma = \frac{q_n}{Gx\beta^2 i_{fg} f_v} \quad (14)$$

4. Calculate $(-dP/dz)_F$ by substituting $(-dP/dz)_v$, • and ς into this equation.

$$\left(-\frac{dP}{dz}\right)_F = (\xi+\varsigma)\left(-\frac{dP}{dz}\right)_v \quad (15)$$

The relative uncertainties of q_n and $(-dP/dz)_F$ become larger for smaller G and x because of smaller static pressure drop and heat transfer rate (Honda et al., 1998; 2000). The propagation of error analyses, based on the above considerations, provide the maximum uncertainties of ± 9% for q_n and ± 17% for $(-dP/dz)_F$.

CONCLUSION

The plan experiment aims to develop a theoretical model for predicting the heat transfer performance and an empirical equation for predicting the pressure drop during condensation of R-407C in a horizontal finned tube. These theoretical model and empirical equation are very important for the development of a condenser that gives the highest performance and the smallest pressure drop. This will, in turn, contribute to the development of compact refrigerating machines and heat pumps with a high coefficient of performance.

ACKNOWLEDGEMENT

I would like to thank Professor Hiroshi Honda at Cooling Technology Laboratory, Institute of Advanced Material Study, Kyushu University collaborated with Monbukagakusho, for his hospitality, encouragement and many helpful discussion.

NOMENCLATURE

A_{fa}	actual free flow area, (m^2)
A_{fn}	nominal flow area, (m^2)
d_i	inner diameter, (m)
d_h	hydraulic diameter, (m)
d_n	nominal diameter, (m)
d_r	fin root diameter, (m)
Fr	Froude number, dimensionless
f_i	friction factor at condensate surface, dimensionless
f_{i0}	friction factor at condensate surface for extreme condition of $v_i \bullet 0$, dimensionless
f_v	friction factor for single phase flow, dimensionless
G	test fluid mass velocity, ($kg/(m^2\ s)$
Ga	Galileo number, dimensionless
g	gravitational acceleration, (m/s^2)
h_f	fin height, (mm)
i	specific enthalpy, (J/kg)
i_{fg}	specific enthalpy of evaporation, (J/kg)
Δl	length of subsection, (m)
m_i	condensation mass flux through condensate surface, ($kg/m^2\ s$)
n	number of fins
Nu	Nusselt number, dimensionless
Nu_d	Nusselt number for tube, nominal surface area basis, dimensionless
$(Nu_d)_g$	Nusselt number for smooth tube, gravity-controlled regime, dimensionless
$(Nu_d)_v$	Nusselt number for smooth tube, vapor shear-controlled regime, dimensionless
Nu_p	Local Nusselt number for fin surface, dimensionless
Nu_{pm}	Average Nusselt number for fin surface, dimensionless
P	pressure, (Pa)
P_{in}	static pressure at vapor inlet, (Pa)
Ph	phase change number, dimensionless
Pr	Prandtl number, dimensionless
p	fin pitch, (mm)
Q_b	heat input to boiler
Q_l	heat loss from boiler
ΔQ	heat transfer rate in subsection
q_n	heat flux based on nominal surface area, (W/m^2)
Re	Reynolds number, dimensionless
T	temperature, (K)

T_c	cooling water temperature, (K)
T_s	saturation temperature, (K)
T_w	wall temperature at fin root, (K)
T_{wm}	average wall temperature of subsection, (K)
u	axial velocity, (m/s)
u_v	actual vapor velocity, (m/s)
u_{vs}	superficial vapor velocity, (m/s)
v_i	suction velocity at condensate surface, (m/s)
X	vapor mass quality, dimensionless
x_{out}	vapor mass quality at tube exit, dimensionless
X_{tt}	Lockhart-Martinelli parameter, dimensionless
z	distance measured from vapor inlet, (m)

Greek symbols

α	heat transfer coeffisient, (W/m^2 K)
β	void fraction, dimensionless
γ	helix angle, (rad)
σ	condensate film thickness (mm)
ς	parameter, dimensionless
η	parameter, dimensionless
θ	fin apex angle (rad)
μ	dynamic viscosity (Pa s)
ν	kinematic viscosity (m^2 /s)
•	parameter, dimensionless
•	density (kg/m^3)
$•_F$	wall shear stress based on nominal surface area (N/m^2)
$•_M$	wall shear stress accounting for momentum change due to condensation, (N/m^2)
φ	circumferential angle measured from tube top (rad)

Subscripts

F	friction component
g	gravity-controlled regime
in	vapor inlet
l	condensate
M	momentum component
n	average evaluation
out	condensate exit
s	saturation or superficial
v	vapor, also vapor shear-controlled regime

REFERENCES

Bergles AE. 1978. *Enhancement of Heat Transfer*. Hemisphere Publishing Corp., New York.

Cavallini A, De Col D, Doretti L, Longo GA, Rossetto L. 2000. Review Paper: Heat Transfer and Pressure Drop During Condensation of Refrigerants Inside Horizontal Enhanced Tubes. *Int J Refrig.*; 23: 4-25

Ebisu T, Fujino H, Torikoshi K. 1998. Heat Transfer Characteristics and Heat Exchanger Performances for R-407C Using Herringbone Heat Transfer Tube. *Proc Int Refrig Conf Purdue*. pp. 343-8.

Fujii, T. 1995. Enhancement to Condensing Heat Transfer - New Development. *J. Enhanced Heat Transfer*; 2: 127-137.

Haraguchi. 1994. *Study on Condensation of HCFC22, HFC134a and HCFC123 Inside Horizontal Tubes*. Doctoral Eng. Thesis. Kyushu University.

Honda H, Nozu S, Katayama H, Nakata H. 1998. Condensation of A Refrigerant CFC11 In Horizontal Micro-Fin Tubes (Proposal of a Correlation Equation for Frictional Pressure Gradient). *Experimental Thermal and Fluid Science*; 18:82-96.

Honda H, Nozu S. 2000. Condensation of Refrigerants in Horizontal, Spirally Grooved Microfin Tubes: Numerical Analysis of Heat Transfer in the Annular Flow Regimes. *J. Heat Transfer*; 122: 80-91.

Incroperra FP, DeWitt DP. 1985. *Fundamental Heat and Mass Transfer*. Second Edition. John Willey and Son.

JSME. 1982. *JSME Data Book, Thermophysical Properties of Fluids*. JSME. Tokyo.

Kuo CS, Wang C. 1996. Horizontal Flow Boiling of R-22 and R-407C in a 9.52 mm Micro-Fin Tube. *App. Ther. Eng.*; 16: 719-731.

Miyara A, Nonaka K, Taniguchi M. 2000. Condensation Heat Transfer and Flow Pattern Inside A Herringbone-Type Micro-Fin Tube. *Int J Refrig.*; 23: 141-152.

Muzzio A, Niro A, Arosio S.1998. Heat Transfer and Pressure Drop During Evaporation and Condensation of R-22 Inside 9.52-mm O.D. Microfin Tubes of Different Geometries. *J. Enhanced Heat Transfer*; 5: 39-52

Wijayanta AT. 1996. *Air Conditioner for Pharmaceutical Industry - A Designation*. Thesis of Engineer Degree. Mechanical Engineering Department, Gadjah Mada University, Yogyakarta.

Wijayanta AT. 1994. *The Overall Heat Transfer Coefficient of Oil Refinery Heat Exchangers-A Recalculation*. A Practical Work Report in Oil and Gas Training Centre; Cepu, Central Java.